Article

Tribological Investigation of the Surface Protective Layer-Forming Effect of a Nano-Sized Yttria–Silica Mixture as a Lubricating Oil Additive

Ádám István Szabó [1,*], Attila Csík [2], Tamás Fodor [2], Kálmán Vad [2], Márk Marsicki [1] and Álmos Dávid Tóth [1]

[1] Department of Propulsion Technology, Széchenyi István University, H-9026 Győr, Hungary; toth.almos@sze.hu (Á.D.T.)

[2] HUN-REN Institute for Nuclear Research, H-4026 Debrecen, Hungary; csik.attila@atomki.hu (A.C.); fodor.tamas@atomki.hu (T.F.); vad.kalman@atomki.hu (K.V.)

[*] Correspondence: szabo.adam@sze.hu

Abstract: Nanoparticles exhibit diverse effects when added as additives to oily medium, enhancing tribological properties and surface characteristics. Studies have shown that many oxide ceramic nanoparticles improve friction and wear, while mixtures also demonstrate favorable tribological properties. This study explores the tribological effect of an yttria–silica (Y_2O_3, SiO_2) nanoparticle mixture in a Group III base oil medium. The results reveal that the yttria–silica mixture significantly reduces friction (-8–17%), mean wear scar diameter (-32%), and wear volume (-94%), while increasing load-bearing capacity ($+114\%$) by creating a durable boundary layer. Observations from scanning electron microscopy revealed the original surface is protected. EDX analyses highlight the boundary layer's elemental composition, which is high in yttrium, silicon, and oxygen and found in higher areas. XRD analysis could not detect the yttria nanoparticle additive within the boundary layer, suggesting that it fragmented due to sliding stress, resulting in an amorphous structure for the new boundary layer. TEM imaging confirmed that the boundary layer thickness is 40–45 nm. These findings demonstrate significant potential for industrial applications in developing advanced, high-performance lubricants for demanding mechanical systems.

Keywords: boundary layer; yttria; tribology; wear; silica; friction

1. Introduction

Nanoparticles can achieve different effects in the form of an additive added to the base oil, and these can be divided into two groups. These two groups are mechanisms with a direct effect on the improvement of lubrication properties and the surface improvement effect. The first group includes the rolling/ball bearing and protective film effect, whereas in the case of the rolling bearing effect, the nanoparticles roll between the friction surfaces. In the case of the protective film effect, the rubbing surfaces are coated with nanoparticles and wear is inhibited. The second group includes the repair and polishing effect. In the case of the repair effect, the nanoparticles fill the grooves of the surface and thus can compensate for the mass loss. In the case of a polishing effect, nanoparticles can reduce the roughness of the lubricating surface [1].

Seyed Borhan Mousavi and his colleagues investigated the effect of nanoparticles in diesel oils. ZnO and MoS_2 nanoparticles were added at various concentrations

(0.1–0.7 wt%) and compared with the results obtained from pure diesel oil measurements. Based on the results, the kinematic viscosity increased at all concentrations, with a more significant increase observed for ZnO nanoparticles. Adding nanoparticles decreased the coefficient of friction (COF) and average surface roughness. The MoS_2 nanoparticles reduced the mass loss of the pins by up to 93%. The oil sample containing 0.7% ZnO increased the flash point and significantly improved the thermophysical properties [2,3]. A $Cu/TiO_2/MnO_2$-doped GO nanocomposite additive was also tested in PAO oil. The results showed that it increased the viscosity index of the oil by 19%; while at an optimal nanoparticle content, it reduced the flash point by 5%, improved the pour point by 24%, and enhanced the anti-wear properties by 46% [4].

Laura Pena-Parás et al. experimented with nanoparticles with fully formulated oils, where CuO and Al_2O_3 nanoparticles were tested at different concentrations. The CuO nanoparticle had an improving effect on friction and wear, increasing the load-bearing capacity. In the case of the Al_2O_3 nanoparticle, an increase in friction and wear was observed [5]. Hernandez Battez et al. also experimented with CuO nanoparticles and tested ZnO and ZrO_2 nanoparticles in PAO 6 type oil. The results also showed a positive effect on friction and wear by adding all three nanoparticles. The best results were shown in the ZnO and ZrO_2 nanoparticle ratio of 0.5 wt% [6]. The tribological improvement properties of ZnO nanoparticles in diesel were also supported by Seyed Borhan Mousavi and Saeed Zeinali Heris [7]. In another experiment by Fatima Leonor Guzman Borda et al., CuO nanoparticles were examined at concentrations of 0.3% and 3% in synthetic polar and mineral oil. The results show that the properties of the synthetic polar oil were not improved by the addition of nanoparticles at either concentration, but the CuO nanoparticles added to the mineral oil improved the friction coefficient and the wear value in both concentrations [8]. The positive effect of CuO nanoparticles was also supported by Y. Choi et al. [9].

S.S. Sanukrishna et al. investigated the effects of SiO_2 nanoparticles as a lubricant additive. During the tests, it was established that the nanoparticles increased the heat transfer coefficient and decreased friction and wear, and the optimal concentration was established at 0.4 wt% [10]. Yashvir Singh et al. reported that adding SiO_2 nanoparticles to an epoxidized Madhuca indica oil increased viscosity and flash point but decreased its pour point. In addition, it also reduced the coefficient of friction and the amount of wear [11]. Meena Ladd and Vijay Kumar S. Jatti tested the TiO_2 nanoparticles in motor oil, and the results proved the positive effect of the nanoparticles, as they reduced the coefficient of friction and wear and supported the excellent solubility of the TiO_2 nanoparticles and their adequate stability [12]. Thottackad et al. conducted experiments with surface-modified CeO_2 nanoparticles in coconut, paraffin, and motor oil. The experimental results show that the friction values and wear decrease as the concentration increases. Still, there is an optimal concentration where the friction and wear values are minimal and then increase again. In addition, they advise that surface activation reduces the sedimentation rate and the extent of agglomerations [13].

Steven J. Thrush et al. conducted experiments with ZrO_2 nanoparticles regarding the process of tribofilm formation, where they tested the oil mixture at 50, 75, and 100 °C in a 2 h measurement range. During the experiments, it was established that the growth rate of the tribofilm is facilitated by the higher temperature and that the tribofilm is much more robust at higher temperatures. In addition, during the measurement process, the tribofilm layer is the thickest in the initial stage of the measurements. Then, the layer starts to thin at low temperatures, at 50 and 75 °C in their experiment. During a 2 h measurement process, this thinning occurred at around 20 min. At 100 °C, the tribofilm formed faster than during the other two measurements and showed a standard thickness, making it more robust. The measurement at 75 °C was repeated by increasing the concentration, and it

can be said that with the increase in concentration, the growth rate and robustness of the tribofilm also increased compared to the measurement with a lower concentration [14]. Kato et al. investigated the tribofilm layer created by oxide nanoparticles. During the experiments, it was confirmed that the tribofilms are generated through the tribosintering of the oxide nanoparticles. It was found that the slight wear on the surfaces is due to the rapid sintering rate of the oxide particles. The sintering rate is also influenced by the oxygen diffusion coefficient in the oxide particles and the particle diameter. The higher the diffusion coefficient of the oxide particle, the faster the tribofilm can be formed, and the wear transition can take place over a short sliding distance [15]. Xiangyu et al. showed the low-friction tribofilm-forming abilities of silica nanoparticles with linear oscillating tests [16]. Dong et al. developed a tribofilm with favorable tribological properties using silica-containing attapulgite nanopowder. Their study demonstrated that silica nanoparticles positively influence the strong bonding between the tribofilm and the metal matrix [17]. Feng et al. also found that silica nanoparticles added to the lubricant become one of the main components of the tribofilm during tribological experiments. The role of silica nanoparticles includes building the tribofilm, strengthening it, binding other materials in the boundary layer, and thereby contributing to the development of favorable tribological properties [18]. The tribofilm reinforced with attapulgite nanopowder can endure high loads [19].

Yttria as a potential nano-additive in lubricating oils is not a primary focus in current research, with very few studies published. The authors have previously examined the tribological effects of yttria-reinforced nanolubricants, reporting favorable friction and wear-reducing impact [20]. They demonstrated that yttria nano-additives incorporate into the metal surface through a plastic deformation interaction, forming an anti-wear boundary layer [21]. Another series of investigations established that in the presence of overbased calcium sulphonate, yttria nano-additives create a solid, dark boundary layer that protects the original surface, withstands extreme pressure and drastically reduces component wear [22].

Surinder Kumar and his colleague Rajesh Kumar attempted to blend two oxide nanoparticles into EP 140 gear oil to achieve improved properties compared to the oil without additives and the individually added oxide nanoparticle blends. The oxide nanoparticles used were CuO and TiO_2 nanoparticles. The final result of the experiment was that nanoparticle oils mixed in different concentrations could improve the friction coefficient, the amount of wear, and the load-bearing capacity compared to the base oil and the nanoparticle oils mixed separately [23]. Jérôme et al. summarize a study demonstrating how oxide ceramic nanoparticles can exhibit plastic properties within a tribological system. Using ultrafine ceramic nanopowders, micro- and nanostructures can be created that, due to their transformation-induced plasticity properties, possess enhanced mechanical characteristics, such as strength, toughness, and elasticity [19]. The favorable tribological properties of the transformation-toughened boundary layer in oxide ceramics are explained by pseudoplasticity behavior [24].

Based on the literature review, yttrium(III) oxide nanoparticles have the potential to form a strong and tribologically effective boundary layer, particularly when enhanced by the addition of silicon dioxide nanoparticles. Surface modification of the nanoparticles with ethyl oleate improves the tribological properties of Group III base oil, resulting in reduced friction and wear by forming a robust tribofilm. This study tests the hypotheses that the combined use of an yttria–silica nanoparticle mixture can enhance tribological performance by creating a strong boundary layer (1); this boundary layer contributes to improved load-bearing capacity, reduced friction, and wear in a Group III base oil (2).

This research aims to determine the properties and behavior of the tribological protective layer formed by adding yttrium(III) oxide and silicon dioxide nanoparticles to base

oil. Key objectives include reducing friction, minimizing wear, and providing a detailed analysis of the protective layer's structure and composition using various surface analytical and thin-film analysis techniques.

The novelty of this paper lies in the first-time combined application of yttrium(III) oxide and silicon dioxide nanoparticles in a single base oil with ethyl oleate surface modification. This approach aims to create a boundary layer with properties that significantly reduce friction and wear. The study uniquely demonstrates how the structural and chemical characteristics of the protective layer and the wear mechanism contribute to enhanced tribological performance.

2. Materials and Methods

During the research, two oxide nanoceramics, yttrium oxide and silicon dioxide nanoparticles, were used. These ceramics were manufactured and shipped from the United States by Sigma-Aldrich (St. Louis, MO, USA). Regarding the particle size of the nanopowders, both particle sizes are below 100 nm (see summary in Table 1). Yttrium oxide is a nanoceramic with a particle size of less than 50 nm and more than 99% purity. Silica nanoceramics have a purity greater than 99.5% and a nanoparticle size between 10 and 20 nm. The mentioned nanopowders were added to a Group III type base oil, a mixture of C_{20}-C_{50} hydrocarbons produced using hydrocracking. The base oil was produced in Hungary by MOL-LUB Kft. at its site in Almásfüzítő, and then shipped.

Table 1. Material properties of the used nanoparticles.

Material	Purity [%]	Average Particle Diameter [nm]	Density [g/cm^3]	Crystal Structure
Silicon dioxide (SiO$_2$)	>99.5	10–20	5.89	Amorphous
Yttrium(III) oxide (Y$_2$O$_3$)	>99	<50	5.01	Body-centered cubic

The oxide nanoparticles used in the experiments underwent surface modification using a previously examined ethyl oleate method by the authors, which was validated on silica nanoparticles [25]. This procedure is necessary so that the oxide nanoparticles do not agglomerate. Agglomerations are visible and have a detrimental effect on the oil sample. Larger agglomerations cannot dissolve completely in the oil, so the concentration ratio in certain places of the oil sample will not be appropriate. At the same time, irrelevant measurement results are returned. During the surface modification, a specific coating is created on the surface of the nanoparticles, which protects the particles from agglomeration. In the present research, the nanopowders underwent surface modification with ethyl oleate. This process requires nanopowder, 90% oleic acid, and 99.6% ethyl alcohol, along with their precisely measured amounts. The amount of unmodified nanopowder added is 0.8 g, the amount of oleic acid is 0.1 g, and the amount of ethyl alcohol added is 65 g. After mixing, place on a magnetic stirrer and stir at 75 ± 5 °C for 2 h. This temperature range is ideal for the reaction of ethyl alcohol and oleic acid, where ethyl oleate is formed and coats the surface of the nanoparticles. Care must be taken so that the mixture's temperature cannot rise above 80 °C, as the ethyl oleate resulting from the reaction of oleic acid and ethyl alcohol burns, requiring special attention. After 2 h, the alcohol cannot evaporate completely, so complete evaporation must be achieved by placing it in a drying cabinet. The internal temperature of the drying cabinet is 80 °C, which is precisely the temperature at which the ethyl oleate does not burn. The surface-modified nanoparticles must be left in the drying cabinet until they are completely dry, and then the surface-modified nanoceramic can be used. This process was carried out with both nanoceramics.

After the surface modification, the oil sample was produced, which uses surface-activated nanoceramics. The selected Group III base oil and toluene were selected, which promote the monodisperse system. After surface activation, the particles have different sizes and have a polydisperse effect in the oil. Adding toluene to the nanoparticles results in a more uniform size distribution, breaking the van der Waals bonds between agglomerates and promoting homogeneous dispersion. The preparation of the oil sample requires accurate calculation, and to achieve the desired concentration, it is also essential to dose the necessary materials for the preparation of the oil sample with a high degree of precision. The desired oil sample concentration can be fully achieved by fulfilling these two conditions. After calculating the required quantities, the exact quantities were measured with a weighing scale with an accuracy of thousandths. 0.5 wt% yttrium oxide and 0.5 wt% silicon dioxide were added to the Group III base oil for these experiments. After measuring, a magnetic stirrer stone was placed in the oil sample. Then, it was stirred for 18 h on a magnetic stirrer to evaporate the toluene, since toluene only helps reach the monodisperse state. Thus, no harmful effects can be experienced after its evaporation. After 18 h, to achieve complete homogeneity, it was placed in an ultrasonic cleaner for 15 min at a temperature of 50 °C, since sedimentation and, thus, smaller agglomerations may still occur after surface activation and adding toluene. The ultrasonic cleaner breaks the remaining van der Waals bonds between them and then puts on the mixer again for 5 min. The complete homogenized state is achieved, and the oil sample is ready for measurement.

The kinematic viscosity of the prepared lubricant samples was tested independently with an Anton Paar SVM 3001 type viscometer at temperatures of 40 and 100 °C. The viscometer enables the measurement of the kinematic viscosity, and the density of the selected temperatures automatically calculates the dynamic viscosity.

Standardized ball and disk specimens were used for the tribological analysis of the prepared lubricant samples. The ball and disk specimens correlate with the ISO 19291:2016 standard [26]. The oscillating Ø 10 mm ball specimens were made of DIN 100Cr6 steel (1.3505 material) with a material hardness of 60 ± 2 HRC. The contact surface of this specimen is prepared for a R_a value of 0.025 ± 0.005 μm. The non-moving disk specimens (Ø 24 mm × 7.9 mm) were also made of DIN 100Cr6 material (1.3505). Still, their material was vacuum arc remelted with spherodized and annealed heat treatment to obtain globular carbides. Their hardness was between 62 ± 1 HRC, and their contacting surfaces were first grinded, followed by lapping with the following parameters: R_a between 0.035 and 0.05 μm and R_Z between 0.5 and 0.65 μm. These testing specimens were always cleaned in an ultrasonic cleaner with brake disk cleaner at 50 °C for 15 min before and after the tribological test to ensure their equal starting conditions before the tribometer measurements and microscopical analysis.

The tribological tests were executed with an Optimol SRV®5 tribometer. This equipment also correlates with the ISO 19291:2016 standard [26] and is widely used for these investigations [27]. The cleaned testing specimens and the homogenized lubricant samples were placed in the tribometer accordingly. The self-developed testing program consists of three steps: (1) preheating up to the required 100 °C temperature and preloading up to 50 N normal force; (2) a short, 30 s step on 50 N load to ensure the minimum required lubricant film between the contacting surfaces; (3) a main step, which lasts 2 h on 100 N load to ensure proper time for the running-in processes and to enable to measure the stabilized friction coefficient at the end of the test, and to produce measurable wear on the contacting surfaces. During the whole test, a constant oil flow rate of 225 mL/h was realized with the help of a peristaltic pump, and the lubricant was preheated up to 100 °C separately from the ball and disk specimens. Static friction (SF) was measured at the dead centers. Based on data collected through high-speed data acquisition, the friction absolute integral (FAI) over

the entire stroke was determined using integral calculation, characterizing the friction across the whole stroke length. During the evaluation, we used Microsoft Excel software with its function library. The results of 12 reference measurements and 4 nanolubricant measurements were used to calculate and display the averages and standard deviations.

A thorough microscopical analysis of the worn surfaces always followed the tribological experiments. A Keyence VHX-1000 (Keyence International, Mechlin, Belgium) digital microscope was used to document the wear scars on the surfaces and measure their dimensions. The mean wear scar diameter values were always calculated according to the correlating ISO 19291:2016 standard [25]: two wear scar diameter values were measured on the surface of the ball specimen, one parallel and one perpendicular to the sliding direction, and their average was considered as the mean wear scar diameter (MWSD). Furthermore, a Leica DCM 3D confocal microscope was also used to digitalize the worn surface of the disk specimens to define the missing wear volume: the whole wear scar, including a significant amount of non-worn surface area, was digitalized firstly, the visible wear scars were determined by hand. Next, the program calculates the average height of the non-worn surface area using the least squares method. Then, the volume inside the defined worn area which is under this average height was calculated by the software itself.

The Rigaku SmartLab (Rigaku Corporation, Tokyo, Japan) diffractometer was used to perform X-ray diffraction (XRD) measurements to obtain crystallographic information from the as-prepared and treated samples. Diffraction patterns were recorded using CuK-alpha irradiation with wavelength $CuK_\alpha = 0.154$ nm. Scans were performed in theta–2theta scanning geometry, and the X-ray tube was operated at 200 mA and 45 kV. Diffraction patterns for Y_2O_3 and SiO_2 powder were measured between $2\Theta = 19$ and $95°$ degrees in the Bragg–Brentano configuration.

In the case of the treated sample, the surface was measured with a parallel beam (PB) in a grazing-incidence configuration to increase the sensitivity. Different low angles were used, which allowed for depth profiling of the near-surface layer of the sample.

Microscopy images revealed the morphology and surface structure of the powders and samples (as received and treated). The samples were investigated with a dual-beam scanning electron microscope (SEM) type Thermo Fisher Scientific-Scios 2 (FIB-SEM, Waltham, MA, USA). In the case of powder, the microscope was operated at a low accelerating voltage (5 keV) and current (50 pA) to avoid surface charge accumulation. Applying such low energy and short working distance allows us to study the surface morphology of insulating powder samples without coating them with a gold layer. The advantages of low acceleration are that it can result in a lower penetration depth of the accelerated electrons, which decreases the interaction volume [28]. The secondary electrons generated near the surface in the reduced value can easily escape, which increases the secondary electron yield.

Due to low acceleration voltage, the specimen current can equal zero because the incoming and outgoing currents will be the same. This means that no electric conductivity of the specimen is required to eliminate the charge accumulation, and insulation materials can be studied without applying a conductive coating layer, which may modify the morphology of the surface. The microscope also has a Bruker-type detector for energy-dispersive X-ray (EDX) analysis.

The gallium ion source built into the microscope was applied to thin the sample for further transmission electron microscopy (TEM) analysis. TEM-lamella has been prepared and transferred to the JEOL (Tokyo, Japan) 2000 FX-II type microscope for a cross-sectional study of the near-surface part of the treated sample.

3. Experimental Results

The prepared and homogenized nanolubricant was first analyzed with the viscometer, and the Group III base oil was used as a reference. The results of the kinematic viscosity

and density at 40 and 100 °C temperatures are summarized in Table 2. It is visible that there is no significant difference in the kinematic viscosity and density between the two lubricant samples; the difference is within 1%. The tiny increase in density can be defined in the yttria and silica-containing samples, and the presence of the nanoparticles can explain this result. It correlates with the density values of the neat components because the silica and yttria nanoparticles have a significantly higher density than the neat Group III type base oil, three times and six times higher, respectively. But this density increase is also under 1%. It can be observed that the flowing properties of the prepared nanolubricant did not change significantly.

Table 2. Kinematic viscosity and density values of lubricant samples at two temperature values.

Lubricant	Kinematic Viscosity [mm^2/s]	Density [g/cm^3]
Group III base oil	20.259 (at 40 °C) 4.373 (at 100 °C)	0.8225 (at 40 °C) 0.7848 (at 100 °C)
Group III + 0.5% Y_2O_3 + 0.5% SiO_2	20.439 (at 40 °C) 4.494 (at 100 °C)	0.8253 (at 40 °C) 0.7888 (at 100 °C)

3.1. Frictional Results

Figure 1 illustrates the measured friction coefficient values of the lubricant samples during the tribotests. It is visible that the measurable frictional losses were reduced in the presence of the nanoparticles. The friction absolute integral (FAI) values decreased by 8%, and the static friction (SF) was reduced by 17%. It can also be observed that the dispersion of friction results is significantly lower with the yttria–silica nano-additive mixture compared to the reference, suggesting the formation of a stable tribofilm on the surface. Applying the yttria–silica nanoparticle mixture as a mild dynamic friction-reducing and significantly static friction-reducing additive holds real potential.
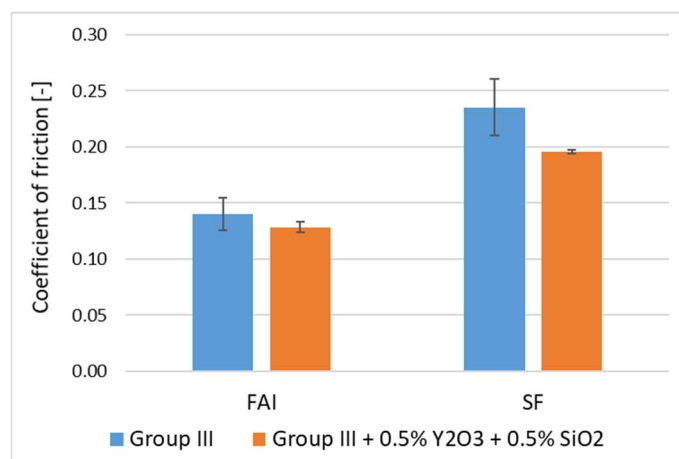

Figure 1. Friction coefficient comparison of the two investigated lubricant samples: the values were selected from the stabilized phase of the measurements.

3.2. Wear Results

The acquired digital microscope images of the worn surfaces of the disk specimens can be seen in Figure 2. The significant wear reduction is visible: the wear scar is much narrower and shiny. Most initial surface roughness grooves are also visible inside the wear scar.

Examining the average wear diameter of the ball, it was found that using nanoceramic additives reduced mean wear scar diameter by 32% (see Figure 3). Consequently, the load-bearing capacity of the surface significantly increased. disks tested with the reference

lubricant operated at an average contact pressure of 388 MPa by the end of the tests. In contrast, using nano-reinforced lubricant formed a surface boundary layer, allowing for a calculable contact pressure of 831 MPa, representing a 114% improvement. It can be stated that the application of the yttria–silica nanoparticle mixture as an extreme pressure additive holds promising potential.
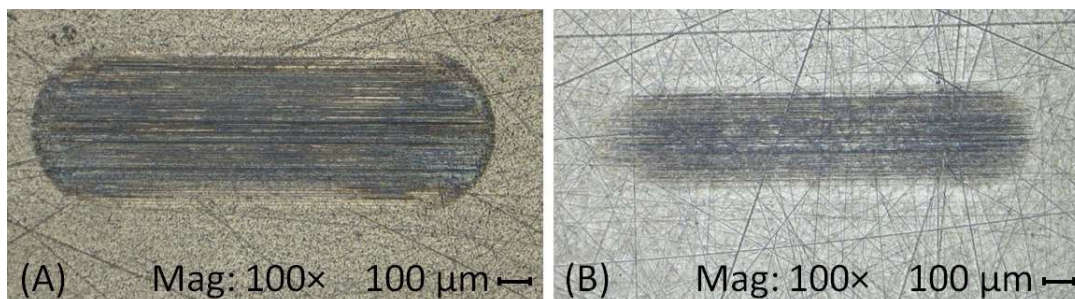

Figure 2. Acquired digital microscope images about the worn surfaces: (**A**) Group III base oil under 100 N; (**B**) Group III + 0.5% Y_2O_3 + 0.5% SiO_2 tested under 100 N load.
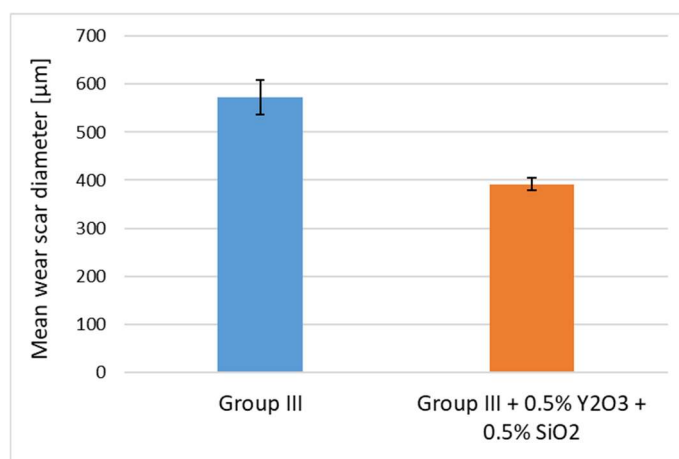
Figure 3. Mean wear scar diameter comparison of the two investigated lubricant samples.

Figure 4 shows the disk wear volume test results, comparing the reference and the lubricant sample with yttria–silica nanoparticle additives. The results indicate that using the nanoceramic mixture reduced wear by an average of 94%. This demonstrates that the yttria–silica nanoceramic mixture may have significant potential in applying anti-wear additives.
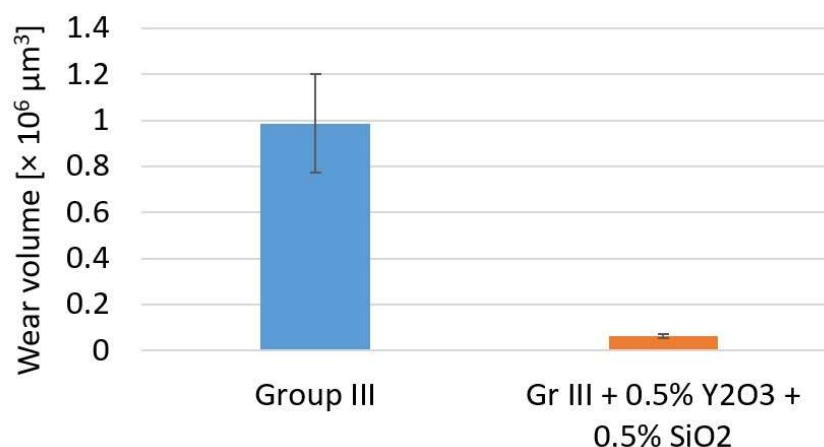

Figure 4. Wear volume comparison of the two investigated lubricant samples.

3.3. Surface Analysis

Figure 5 shows the electron microscopy images of the wear on the disk test specimen tested with the nanoparticle-containing lubricating oil. In the top row, images (a) are from the disk's center (area with the highest relative speed), while the bottom row displays images taken at the disk's dead center (ball stopping point). The SEM images on the left column provided the basis and location for the EDX analysis: the middle photos show the intensity of the yttrium element on the worn surfaces in yellow, while the right images show the intensity of the silicon element in blue. The more vivid and abundant the color, the higher the concentration of the examined element.
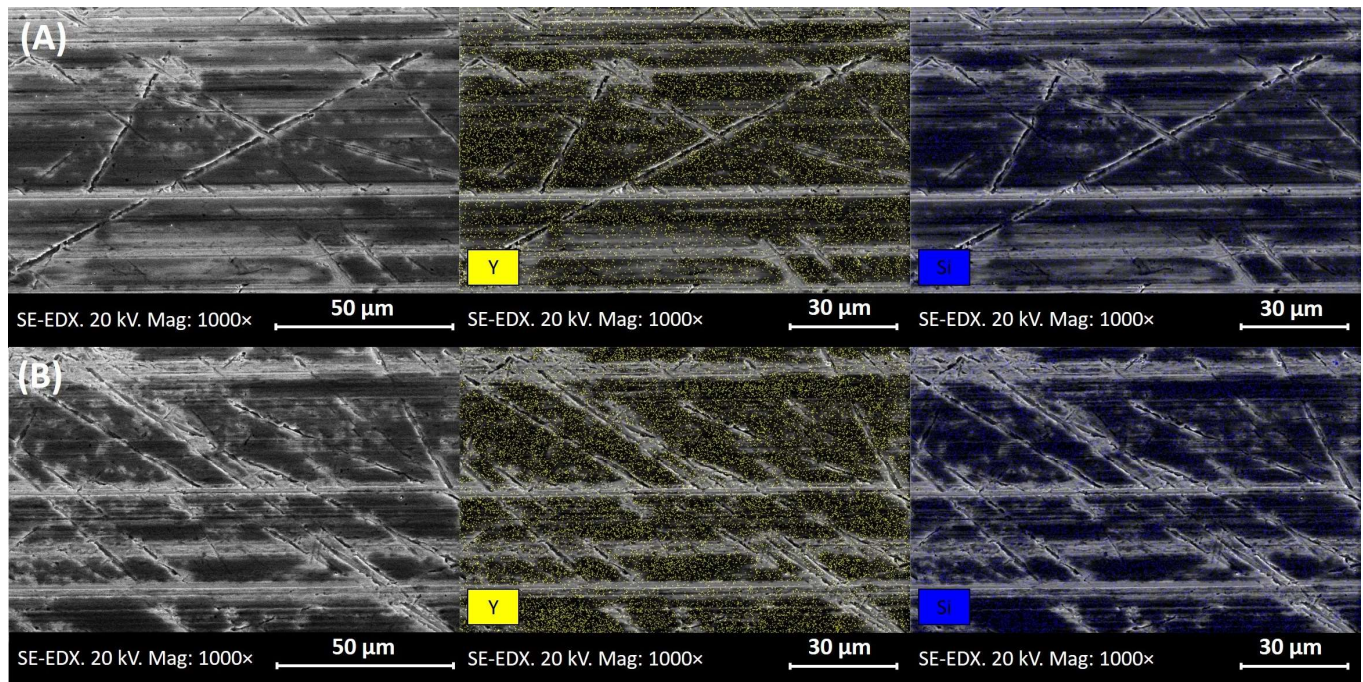
Figure 5. SEM images of disk wear marks: (**A**) at the center point of the wear track; (**B**) at the dead center of the wear track. The location and intensity of yttrium and silicon elements on the wear marks are indicated by yellow and blue colors, respectively.

The primary purpose of the SEM images is to examine the topography of the worn surfaces to identify the types of wear present. It can be concluded that abrasive wear is the dominant type in both the worn center point and dead center. The characteristic, motion-parallel long grooves of abrasive wear are observable in the images. Additionally, despite the fine lapping of the disk specimen with low R_a and R_z values, the average wear depth does not reach the depth of the original surface roughness. A significant amount of the original surface's grooves and texture remain. With their excellent oil-carrying capacity, the deep grooves remaining on the original surface may have reduced friction (particularly the additional grooves remaining at the dead center, contributing to a lower static friction value).

It can also be observed that wear is deeper in the center of the disk (A), where only the deepest roughness grooves remain, in contrast to the dead center region (B). The yttria nano-additive has plastically deformed the higher surface regions [21], with the extent of deformation being higher in the center. The plastically deformed surfaces appear typically flat and show darker coloration in the SEM images. The grooves and depressions on the surface appear to be bright areas. The EDX results indicate that the dark, plastically deformed regions generally show higher intensity and incorporation of the nanoparticle elements than the bright, deep areas [22].

After the treatment, the sample was investigated using several analytical methods. First, the treated part of the sample was measured using the energy-dispersive X-ray (EDX) method to confirm the presence of the applied material on the surface. EDX measurement affirms that silicon and yttrium have been found on the treated surface (see Figure 6).
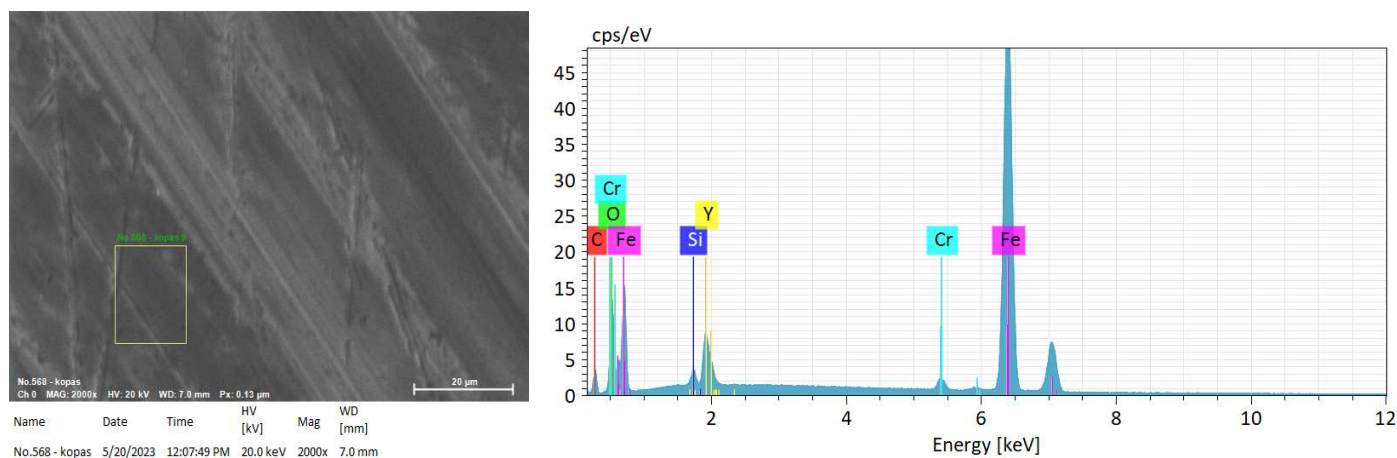

Figure 6. Result of EDX measurement as a spectrum. The inset shows the treated surface part; the measurement was performed in the dark, worn area marked with the yellow box.

The EDX quantification results of the surfaces show the main components, alloying materials, and investigated elements of the DIN 100Cr6 disk test specimen in weight percentage [wt%], as seen in Table 3. A significant amount of carbon is on the unworn surface, which can be attributed to oil derivatives bonded to the surface. No yttrium is found on the unworn surface, and silicon is present at 0.39 wt%. Yttrium is not found in the oil or test specimens, so its exclusive source is the yttria nano-additive. However, when examining worn surfaces, it is evident that areas with a dark boundary layer in the SEM images contain significantly more elements derived from the nano-additive than others. The dark boundary layer contains 2.63 wt% yttrium and 0.89 wt% silicon, and the oxygen content is exceptionally high at 9.79 wt%, suggesting that the nanoparticles are still predominantly present on the surface in oxidized form. The iron content is lower in areas covered by the dark boundary layer, as the tribofilm partially covers the base metal matrix. Similar trends are observed in the bright regions of the wear marks but to a lesser extent: Y = 0.34 wt%; Si = 0.49 wt%; O = 3.33 wt%. Therefore, the nanoparticles are primarily constituent elements of the higher, plastically deformed dark boundary layer.

Table 3. Quantifying elements on unworn and worn surfaces in weight percentage [wt%].

Area	Iron	Chromium	Silicon	Oxygen	Carbon	Yttrium
Unworn reference	89.88	1.28	0.37	0.05	8.42	0.00
Worn 'dark'	76.00	1.12	0.89	9.79	9.56	2.63
Worn 'light'	86.61	1.38	0.49	3.33	7.85	0.34

Both Y_2O_3 and SiO_2 powder were investigated using SEM and XRD methods. Figure 7A,B show typical images of powders. In the case of Y_2O_3, the powder used for the experiments is made up of closely connected lamellae with a crystalline structure. SEM images of silica nanoparticles show bulk amorphous material with ball morphology particles sticking together into larger chunks.

The concentration of yttrium and silicon is localized to regions where the surface was subjected to tribological stress, enabling tribofilm formation. In untreated areas, yttrium

is absent, as tribofilm development requires the abrasive force exerted by the counter-body. This also explains why nanoparticles are visible in the deformed surface but not in the grooves; the grooves experience minimal force, preventing tribofilm formation. Additionally, any nanoparticles in the grooves do not form strong bonds and are likely removed during ultrasonic cleaning before microscopic analysis. As detected in the EDX analysis, oxygen is an inherent component of the oxide nanoparticles used in the study. Additionally, oxygen is introduced to the surface through tribochemical oxidation processes occurring during the tribological tests. This dual contribution explains its presence in the regions where tribofilm formation is observed.
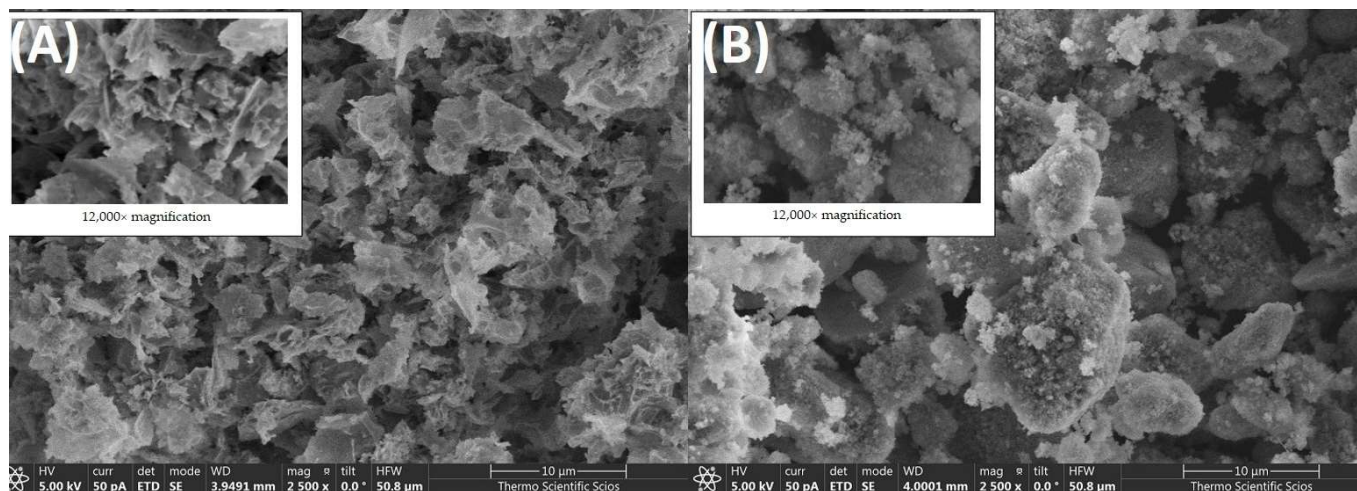
Figure 7. A scanning electron microscopy image was taken from the Y_2O_3 powder on the left (**A**) and the SiO_2 nanopowder on the right (**B**). The insets show a 12,000× magnification of a smaller area.

The XRD measurement has confirmed the crystallinity of the powder. Figure 8A shows the diffraction pattern compared with the database, and the Y_2O_3 crystal structure could be identified with the #PDF00-041-1105 card number. Figure 8B shows the measurement result of the silica powder wherein the powder has an amorphous structure. The crystallite size for applied Y_2O_3 powder was calculated from an X-ray diffraction pattern of strongest reflection with intensity by measuring the full width at half maximum (FWHM). The equation for calculating the crystallite size is given as follows [29,30]:

$$D = \frac{K \cdot \lambda}{\beta \cdot \cos \theta},$$

where K is the Scherrer constant (we used value 0.9), λ is the wavelength of X-ray for diffraction, β is the FWHM of the peak with the highest intensity (in radians), and θ is the measured Bragg angle of the same peak. Based on the calculation, we obtained a value of 12.63 nm for the average crystallite size Y_2O_3 powder.

A surface-sensitive diffraction measurement was performed to study the presumably thin surface layer's structure. Grazing incidence diffraction (GID) [31] is a technique for studying material using small incidence angles for an incoming wave, often making the diffraction surface sensitive. The small incident angle is set near the critical angle, enhancing the sensitivity of the method to surface structures and interfaces. GID is particularly valuable for investigating thin films, multilayers, and surfaces, providing detailed insights into the arrangement of atoms and molecular structures at the material's surface. The method's key advantage lies in probing buried interfaces and thin layers. In this case, four different angles of incidence were used, for which the penetration depth of the X-ray beam

was calculated according to the method described by Henek et al. [32,33], and the data can be seen in Table 4.
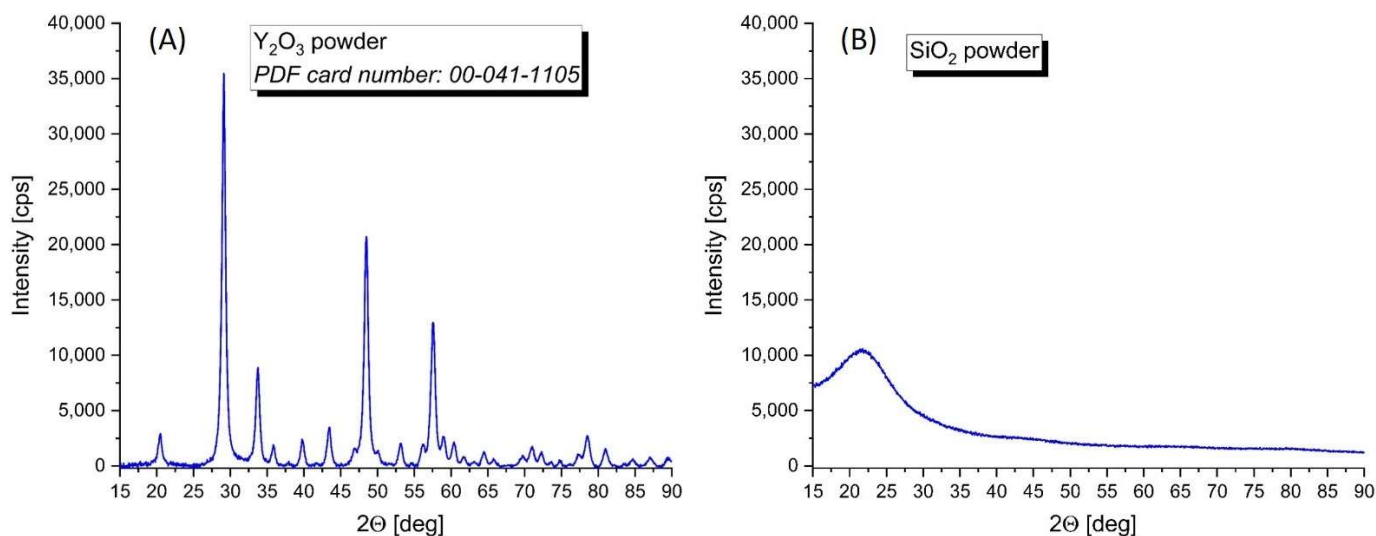

Figure 8. The X-ray diffraction pattern was measured on the Y_2O_3 nanopowder on the left (**A**). The presence of well-defined and sharp peaks confirms the crystallinity of the measured sample. The result of X-ray diffraction measurement on SiO_2 powder can be seen on the right (**B**). A typical diffraction pattern of an amorphous structure can be observed.

Table 4. Calculated penetration depth of X-ray irradiation onto the iron at different incident angles. The calculation was carried out according to reference [33].

Incident Angle, 2Θ [deg]	Penetration Depth [nm]
0.7	43.3
0.9	60.1
1.4	99.4
2.7	197.2

Comparing the results measured at four different angles of incidence, there was no difference in the diffraction patterns measured at various depths. However, if we look at the diffraction pattern measured at an incidence angle of $\omega = 0.7°$, we can see a small intensity peak at 55.3 degrees (see Figure 9). This small peak was not noticeable at higher incidence angles (enlarged diffraction patterns are not presented here). In Figure 9B, the vertical straight lines correspond to the positions of the $Fe_{17}Y_2$ phase reflections, according to the powder diffraction database card number PDF#01-079-5149. As can be seen, many peaks overlap with the base 100Cr6 material. The other intensities are relatively low; however, we can say that this diffraction peak may belong to a $Fe_{17}Y_2$ phase.

From the transmission electron microscope image (see Figure 10), it can be seen that a 40–45 nm layer was formed on the surface of the iron after treatment. To verify the composition of the formed layer, the selected area on the cross-section sample was measured using the EDX method. Figure 10B shows the results of the elemental composition measurement in the area marked in green on the microscopic image. The figure shows that the presence of Si and Y, although with low intensity, can be detected. As the layer thickness is in the range of 40–45 nm during the EDX measurement, the e-beam spot size overlaps with the bulk substrate and the platinum-protecting layer. Therefore, metallic elements are visible in the spectrum; Ga also appears due to the cross-sectional sample preparation made using the focused ion beam (FIB) method.
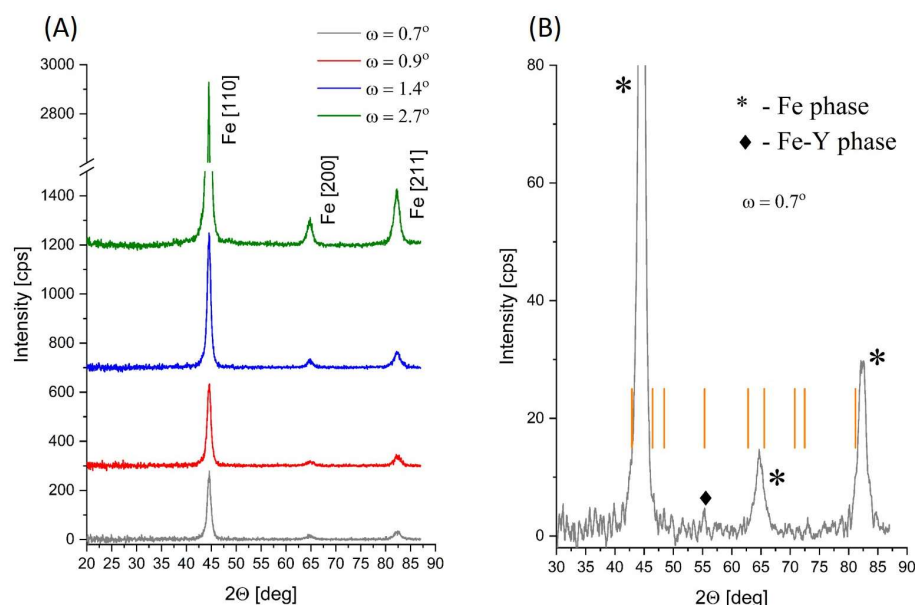
Figure 9. (**A**) Result of grazing diffraction measurement on the treated sample at four incident angles. (**B**) Enlarged image of the diffraction pattern at 0.7° incident angle. Vertical straight lines (orange colored) correspond to the peak position of the $Fe_{17}Y_2$ phase from the powder diffraction card numbered PDF#01-079-5149. For the sake of clarity, not all peak positions are shown here.
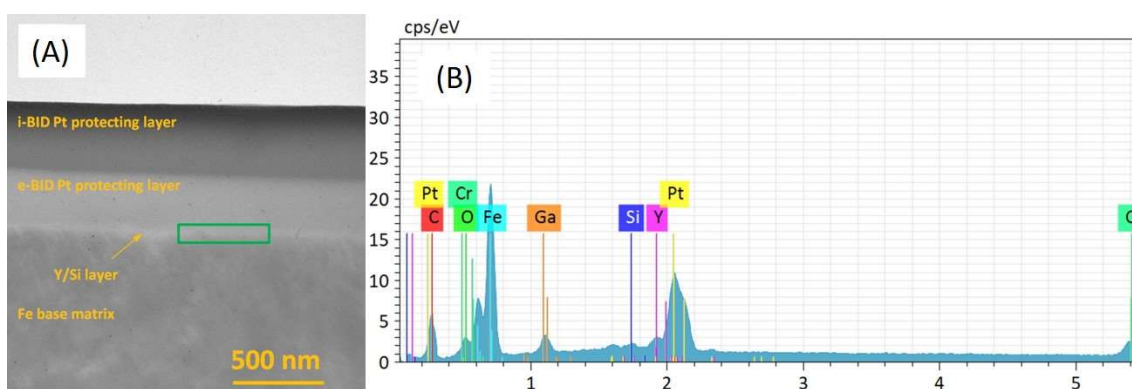

Figure 10. (**A**) Cross-sectional transmission electron microscopy image of the treated sample. The thin white colored line represents the surface layer after the treatment process. (**B**) The result of the composition analysis measurement was carried out in the area marked with the green rectangle.

Based on this direct observation and the result of XRD measurement at a low incident angle, we can say that a Fe-Y phase could have formed at the interface between the iron and the amorphous Y/Si-oxide layer during the treatment. The possibility and conditions for forming the $Fe_{17}Y_2$ intermetallic compound were described by Chenbo et al., whose suitability aligns with the conditions of the applied tribological experimental investigations [34].

The results support the hypothesis regarding the boundary layer-building effect of yttria–silica nanoparticle mixture as lubricant additives and their excellent tribological properties. The findings align with the expectations from the literature review and are consistent with observations from other studies. However, some aspects remain hypotheses based on the available data and require further investigation to confirm. The operation of the yttria–silica nanoparticle additive mixture and the mechanism of yttria nanoparticles may be as follows:

- The yttria–silica nano-additive mixture reduces friction and wear and acts as an extreme pressure additive [20]. However, this effect is primarily attributed to its

boundary layer-forming capability, which creates a mechanically robust and pressure-resistant tribofilm [19].

- The extent of the yttria-reinforced boundary layer is enhanced by adding silica nanoparticles, which aid in binding to the metal surface [17,18].
- In a body-centered cubic crystal structure, dislocation movement is limited, resulting in weak plastic deformation capability, making the structure brittle and rigid. This restricts its ability to absorb energy under bending or sliding stress, as dislocations slide less readily (especially in cold environments) [35].
- Nanoparticles on the surface undergo fragmentation (<50 nm) under sliding stress, causing the crystal lattice to fracture and form an amorphous thin layer of 40–45 nm thickness [24]. This layer is visible in HRSEM images but is challenging for XRD to detect.
- Based on the results and the literature, the yttria–silica layer on the upper surface is hypothesized to adopt pseudoplastic behavior due to its transformation-induced plasticity properties [19]. This behavior contributes to the layer's enhanced mechanical properties and favorable tribological characteristics, but further validation through microstructural investigations and targeted friction tests is necessary.
- Furthermore, it is hypothesized that tribochemical reactions result in the formation of a small amount of $Fe_{17}Y_2$ intermetallic compound in the boundary layer from smaller fragments generated during abrasion or fracturing [34]. Although this phase is consistent with the literature and observed results, it remains speculative and requires confirmation or refutation through additional measurements in future studies.

The novelty of this paper lies in presenting the tribological effects of a lubricant doped with an yttria–silica nano-additive blend, highlighting boundary layer formation. The favorable tribological characteristics observed are all attributable to the yttrium-enriched surface layer identified in electron microscopy images. The paper describes the characteristics of this layer and its likely formation process.

4. Conclusions

This study demonstrates the tribological benefits of using a combined yttria–silica nanoparticle additive in a Group III base oil, emphasizing the significance of boundary layer formation and its impact on friction and wear reduction. Forming a boundary layer with pseudo-plastic behavior illustrates the potential for yttria–silica additives to enhance load-bearing capacity, minimize surface wear, and improve friction characteristics. The tribological results show the effectiveness of the yttria–silica nano-additive mixture:

- Friction reduction was notable, with the FAI values decreasing by 8% and SF by 17%, reflecting the stability of the boundary layer.
- Wear performance showed remarkable improvement, with a 32% reduction in mean wear scar diameter and a 94% reduction in wear volume.
- Load-bearing capacity increased by 114%, with pressure resistance improving from 388 MPa to 831 MPa.

Through surface analytical techniques, several properties of the boundary layer have been identified, which helped in drawing probable conclusions about its formation process:

- The characteristic abrasive wear and the boundary layer that plastically modified the upper part of the wear mark (preserving surface roughness in some regions) are visible in the SEM images.
- Using EDX, it was determined that the protective boundary layer consists of a substantial amount of yttrium (2.63 wt%), silicon (0.89 wt%), and oxygen (9.79 wt%).

- XRD revealed the transformation of crystalline yttria nanoparticles into an amorphous structure, with the possibility of minor Fe-Y phase formation under sliding stress.
- TEM showed the boundary layer thickness to be approximately 40–45 nm.

The importance of this work lies in the novel approach of combining yttria and silica nanoparticles with surface modifications to form a stable, robust tribofilm during a tribological experiment. The results highlight a significant advancement in developing nanolubricants with enhanced properties.

Future research should focus on the nanoscale interactions within the boundary layer, emphasizing chemical bonding mechanisms, the nanostructure, and the long-term stability of the tribofilm under varied operational conditions. Investigating the synergistic and antagonistic effects of nanoparticle interactions and the molecular interactions involved in boundary layer formation and tribochemical reactions is essential. Understanding these processes is crucial for creating stable pseudoplastic boundary layers through nano-additive inclusion. To validate the possible pseudoplasticity observations, future studies should include microstructural investigations and focused friction analysis. These insights could pave the way for designing high-performance lubricants and significantly affect machine design and lubricant development. This study lays a foundation for further explorations into nanolubricants, promising substantial contributions to tribology, surface science, and advanced lubricant formulations.

References

1. Lee, K.; Hwang, Y.-J.; Cheong, S.; Choi, Y.; Kwon, L.; Lee, J.; Kim, S. Understanding the Role of Nanoparticles in Nano-oil Lubrication. *Tribol. Lett.* **2009**, *35*, 127–131. [CrossRef]
2. Mousavi, S.B.; Heris, S.Z.; Estellé, P. Viscosity, tribological and physicochemical features of ZnO and MoS_2 diesel oil-based nanofluids: An experimental study. *Fuel* **2021**, *293*, 120481. [CrossRef]
3. Mousavi, S.B.; Heris, S.Z.; Estellé, P. Experimental comparison between ZnO and MoS_2 nanoparticles as additives on performance of diesel oil-based nano lubricant. *Sci. Rep.* **2020**, *10*, 5813. [CrossRef] [PubMed]
4. Mousavi, S.B.; Pourpasha, H.; Heris, S.Z. High-temperature lubricity and physicochemical behaviors of synthesized $Cu/TiO_2/MnO_2$-doped GO nanocomposite in high-viscosity index synthetic biodegradable PAO oil. *Int. Commun. Heat Mass Transf.* **2024**, *156*, 107642. [CrossRef]
5. Taha-Tijerina, J.; Peña-Parás, L.; Maldonado, D.; Michalczewski, R.; Garza, L.; Lapray, C. Effect of CuO and Al_2O_3 Nanoparticle Additives on the Tribological Behavior of Fully Formulated Oils. *Wear* **2015**, *332–333*, 1256–1261.
6. Hernández Battez, A.; González, R.; Viesca, J.L.; Fernández, J.E.; Díaz Fernández, J.M.; Machado, A.; Chou, R.; Riba, J. CuO, ZrO_2 and ZnO Nanoparticles as Antiwear Additive in Oil Lubricants. *Wear* **2008**, *265*, 422–428. [CrossRef]
7. Mousavi, S.B.; Zeinali Heris, S. Experimental Investigation of ZnO Nanoparticles Effects on Thermophysical and Tribological Properties of Diesel Oil. *Int. J. Hydrogen Energy* **2020**, *45*, 23603–23614. [CrossRef]

8. Borda, F.; Oliveira, S.; Lazaro, L.; Leiroz, A. Experimental Investigation of the Tribological Behavior of Lubricants with Additive Containing Copper Nanoparticles. *Tribol. Int.* **2017**, *117*, 52–58. [CrossRef]

9. Choi, Y.E.; Lee, C.; Hwang, Y.-J.; Lee, J.; Choi, C.; Jung, M. Tribological Behavior of Copper Nanoparticles as Additives in Oil. *Curr. Appl. Phys.* **2009**, *9*, 124–127. [CrossRef]

10. Sanukrishna, S.S.; Shafi, M.; Murukan, M.; Prakash, J. Effect of SiO_2 Nanoparticles on the Heat Transfer Characteristics of Refrigerant and Tribological Behaviour of Lubricant. *Powder Technol.* **2019**, *356*, 39–49. [CrossRef]

11. Singh, Y.; Rahim, E.; Singh, N.K.; Sharma, A.; Singla, A.; Palmanit, A. Friction and Wear Characteristics of Chemically Modified Mahua (*Madhuca indica*) Oil-Based Lubricant with SiO_2 Nanoparticles as Additives. *Wear* **2022**, *508–509*, 204463. [CrossRef]

12. Laad, M.; Jatti, V. Titanium Oxide Nanoparticles as Additives in Engine Oil. *J. King Saud Univ. Eng. Sci.* **2016**, *30*, 116–122. [CrossRef]

13. Thottackkad, M.; Rajendrakumar, P.; Prabhakaran, N. Tribological Analysis of Surfactant Modified Nanolubricants Containing CeO_2 Nanoparticles. *Tribol. Mater. Surf. Interfaces* **2014**, *8*, 125–130. [CrossRef]

14. Thrush, S.; Comfort, A.; Dusenbury, J.; Nautiyal, P.; Elinski, M.; Carpick, R.; Demas, N.; Gould, B.; Han, X.; Wang, X.; et al. Growth and Morphology of Thermally Assisted Sinterable Zirconia Nanoparticle Tribofilm. *Tribol. Int.* **2022**, *175*, 107820. [CrossRef]

15. Kato, H.; Komai, K. Tribofilm Formation and Mild Wear by Tribo-Sintering of Nanometer-Sized Oxide Particles on Rubbing Steel Surfaces. *Wear* **2007**, *262*, 36–41. [CrossRef]

16. Liu, X.; Xu, N.; Li, W.; Zhang, M.; Chen, L.; Lou, W.; Wang, X. Exploring the effect of nanoparticle size on the tribological properties of SiO_2/polyalkylene glycol nanofluid under different lubrication conditions. *Tribol. Int.* **2017**, *109*, 467–472.

17. Wang, D.; Zeng, X.; Feng, N. Tribological behaviors of an attapulgite–graphene nanocomposite as an additive for mineral lubricating oil. *RSC Adv.* **2024**, *14*, 16411.

18. Feng, N.; Xu, Y.; Xu, B.; Gao, F.; Wu, Y.; Li, Z. Tribological Performance of Attapulgite Nano-fiber/Spherical Nano-Ni as Lubricant Additive. *Tribol. Lett.* **2014**, *56*, 531–541.

19. Jérôme, C.; Aléthéa, L.; Helen, R.; Fei, Z.; Pascal, R.; Thierry, D.; Laura, P.; Valter, S.; Vanni, L.; Mike, S.; et al. Forty years after the promise of «ceramic steel?»: Zirconia-based composites with a metal-like mechanical behavior. *J. Am. Ceram. Soc.* **2019**, *103*, 1482–1513.

20. Tóth, Á.D.; Szabó, Á.I.; Rohde-Brandenburger, J.; Kuti, R. Impact of Yttria Reinforced Nanolubricants onto the Tribological Properties. *Hidraulica* **2021**, *3*, 26–33.

21. Tóth, Á.D.; Szabó, Á.I.; Leskó, M.Z.; Rohde-Brandenburger, J.; Kuti, R. Tribological Properties of the Nanoscale Spherical Y_2O_3 Particles as Lubricant Additives in Automotive Application. *Lubricants* **2022**, *10*, 28. [CrossRef]

22. Tóth, Á.D.; Hargitai, H.; Szabó, Á.I. Tribological Investigation of the Effect of Nanosized Transition Metal Oxides on a Base Oil Containing Overbased Calcium Sulfonate. *Lubricants* **2023**, *11*, 337. [CrossRef]

23. Kumar, S.; Kumar, R. Tribological Characteristics of Synthesized Hybrid Nanofluid Composed of CuO and TiO_2 Nanoparticle Additives. *Wear* **2023**, *518–519*, 204623. [CrossRef]

24. Grabowy, M.; Wojteczko, A.; Osada, P.; Wiazania, G.; Pedzich, Z. The Influence of the Phase Arrangement of Atz Composites on Their Wear Rate Under Ball-On-Disc Tests. In Proceedings of the 18th International Conference on Tribology—SERBIATRIB '23, Kragujevac, Serbia, 17–19 May 2023.

25. Tóth, Á.D.; Mike-Kaszás, N.; Bartus, G.; Hargitai, H.; Szabó, Á.I. Surface Modification of Silica Nanoparticles with Ethyl Oleate for the Purpose of Stabilizing Nanolubricants Used for Tribological Tests. *Ceramics* **2023**, *6*, 980–993. [CrossRef]

26. *ISO 19291:2016(E)*; ISO (International Organization for Standardization). Lubricants—Determination of Tribological Quantities for Oils and Greases—Tribological Test in the Translator Oscillation Apparatus. ISO: Geneva, Switzerland, 2016.

27. Patzer, G.; Woydt, M. New Methodologies Indicating Adhesive Wear in Load Step Tests on the Translatory Oscillation Tribometer. *Lubricants* **2021**, *9*, 101. [CrossRef]

28. Erdman, N.; Bell, D.C.; Reichelt, R. Scanning Electron Microscopy. In *Springer Handbook of Microscopy*; Hawkes, P.W., Spence, J.C.H., Eds.; Springer Handbooks; Springer International Publishing: Cham, Switzerland, 2019; pp. 229–318. ISBN 978-3-030-00069-1.

29. Sobhani, E.; Heris, S.Z.; Mousavi, S.B. The Synergistic Effect of Intumescent Fire-Resistive Paint Containing TiO_2 Nanoparticles and Chlorinated Paraffin onto Atmospheric-Metallic Substrates. *ChemistrySelect* **2022**, *7*, e202203513. [CrossRef]

30. Mousavi, S.B.; Heris, S.Z.; Hosseini, M.G. Experimental investigation of MoS2/diesel oil nanofluid thermophysical and rheological properties. *Int. Commun. Heat Mass Transf.* **2019**, *108*, 104298. [CrossRef]

31. Chang, S.-L. Thin-Film Characterization by Grazing Incidence X-Ray Diffraction and Multiple Beam Interference. *J. Phys. Chem. Solids* **2001**, *62*, 1765–1775. [CrossRef]

32. Henke, B.L.; Gullikson, E.M.; Davis, J.C. X-Ray Interactions: Photoabsorption, Scattering, Transmission, and Reflection at E = 50–30,000 eV, Z = 1–92. *At. Data Nucl. Data Tables* **1993**, *54*, 181–342. [CrossRef]

33. Glancing Incidence X-Ray Analysis (GIXA). Available online: https://gixa.ati.tuwien.ac.at/tools/penetrationdepth.xhtml (accessed on 8 November 2024).

34.   Li, C.; Song, Q.; Yang, X.; Wei, Y.; Hu, Q.; Liu, L.; Zhang, L. Experimental Investigation of the Phase Relations in the Fe-Zr-Y
        Ternary System. *Materials* **2022**, *15*, 593. [CrossRef]
35.   Yu-Heng, Z.; En, M.; Jun, S.; Wei-Zhong, H. A unified model for ductile-to-brittle transition in body-centered cubic metals.
        J. Mater. Sci. Technol. **2023**, *141*, 193–198.